AFRL-RH-FS-TR-2014-0047

Computational Modeling Basis in the Photostress Recovery Model (PREMO)

Leon N. McLin
Human Effectiveness Directorate
Bioeffects Division
Optical Radiation Bioeffects Branch

Elharith M. Ahmed
Peter A. Smith
Daniel F. Huantes
Philip A. Tessier
Edward A. Early
TASC, Inc.

September 2014
Interim Report for October 2011 to March 2014

DESTRUCTION NOTICE – Destroy by any method that will prevent disclosure of contents or reconstruction of this document.

Air Force Research Laboratory
711th Human Performance Wing
Bioeffects Division
Optical Radiation Bioeffects Branch
JBSA Fort Sam Houston, Texas 78234

NOTICE AND SIGNATURE PAGE

Using Government drawings, specifications, or other data included in this document for any purpose other than Government procurement does not in any way obligate the U.S. Government. The fact that the Government formulated or supplied the drawings, specifications, or other data does not license the holder or any other person or corporation; or convey any rights or permission to manufacture, use, or sell any patented invention that may relate to them.

Qualified requestors may obtain copies of this report from the Defense Technical Information Center (DTIC) (http://www.dtic.mil).

"Computational Modeling Basis in the Photostress Recovery Model (PREMO)"

(AFRL-RH-FS-TR- 2014 - 0047) has been reviewed and is approved for publication in accordance with assigned distribution statement.

NEMMERS.SCOTT.A.1138135809

Digitally signed by NEMMERS.SCOTT.A.1138135809
DN: c=US, o=U.S. Government, ou=DoD, ou=PKI, ou=USAF, cn=NEMMERS.SCOTT.A.1138135809
Date: 2014.12.16 08:37:05 -06'00'

SCOTT NEMMERS, LT COL, USAF
Branch Chief
Optical Radiation Bioeffects Branch

POLHAMUS.GARRETT.D.1175839484

Digitally signed by POLHAMUS.GARRETT.D.1175839484
DN: c=US, o=U.S. Government, ou=DoD, ou=PKI, ou=USAF, cn=POLHAMUS.GARRETT.D.1175839484
Date: 2015.02.11 08:26:23 -06'00'

GARRETT D. POLHAMUS, DR-IV, DAF
Chief, Bioeffects Division
Human Effectiveness Directorate
711th Human Performance Wing
Air Force Research Laboratory

This report is published in the interest of scientific and technical information exchange, and its publication does not constitute the Government's approval or disapproval of its ideas or findings.

REPORT DOCUMENTATION PAGE

Form Approved
OMB No. 0704-0188

1. REPORT DATE *(DD-MM-YYYY)*	2. REPORT TYPE	3. DATES COVERED *(From - To)*
20-09-2014	Interim	October 2011-March 2014

4. TITLE AND SUBTITLE
Computational Modeling Basis in the Photostress Recovery Model (PREMO)

5a. CONTRACT NUMBER
FA8650-14-D-6519

5b. GRANT NUMBER

5c. PROGRAM ELEMENT NUMBER
0602202F30

6. AUTHOR(S)
Leon N. McLin, Elharith M. Ahmed, Peter A. Smith, Daniel F. Huantes, Philip A. Tessier, Edward A. Early

5d. PROJECT NUMBER
7757

5e. TASK NUMBER
HD

5f. WORK UNIT NUMBER
03-H0BA

7. PERFORMING ORGANIZATION NAME(S) AND ADDRESS(ES)

Air Force Research Laboratory
711th Human Performance Wing
Optical Radiation Branch
JBSA Fort Sam Houston
TX 78234-2644

TASC, Inc.
4141 Petroleum Rd
JBSA Fort Sam Houston
TX 78234-2644

8. PERFORMING ORGANIZATION REPORT NUMBER

9. SPONSORING / MONITORING AGENCY NAME(S) AND ADDRESS(ES)

Air Force Research Laboratory
711th Human Performance Wing
Optical Radiation Branch
JBSA Fort Sam Houston
TX 78234-2644

10. SPONSOR/MONITOR'S ACRONYM(S)
711 HPW/RHDO

11. SPONSOR/MONITOR'S REPORT NUMBER(S)
AFRL-RH-FS-TR-2014-0047

12. DISTRIBUTION / AVAILABILITY STATEMENT
Pending Distribution A: Approved for public release; distribution unlimited. PA Case No: TSRL-PA-15-0029

13. SUPPLEMENTARY NOTES

14. ABSTRACT
A model that predicts the impact of optical radiation on visual function has been developed. The model assesses the impact of glare and glare recovery on performance by tracing the propagation of light from the source to the eye and determining the effect on visual contrast sensitivity. This capability analyzes broadband and extended sources, supports complex visual tasks, and displays a visualization of the post exposure visual recovery process. The model is composed of four components: a scene generation component, an optical source processing component, a glare and flashblindness component, and an identification/recognition component. The scene generation component utilizes an off-the-shelf 3D scene viewer that allows the user to set up a scenario in 3D space and uses the geometry of that scenario to create a perceived scene relative to an observer in the scenario. The optical source processing component propagates the source image to the observer's eye position and computes the retinal distribution of the optical source. The photostress recovery component determines how the optical radiation exposure obscures the visual scene through the process of contrast reduction and how visual sensitivity recovers after the exposure has been terminated. Finally, the identification/recognition component determines the probability of identifying/recognizing a given target at any post exposure point in time.

15. SUBJECT TERMS

16. SECURITY CLASSIFICATION OF:			17. LIMITATION OF ABSTRACT	18. NUMBER OF PAGES	19a. NAME OF RESPONSIBLE PERSON
					Semih Kumru
a. REPORT	b. ABSTRACT	c. THIS PAGE	SAR	30	19b. TELEPHONE NUMBER *(include area code)*
Unclassified	Unclassified	Unclassified			

Standard Form 298 (Rev. 8-98)
Prescribed by ANSI Std. 239.18

This page is intentionally blank

TABLE OF CONTENTS

LIST OF FIGURES

1. INTRODUCTION

1.1 Background

The primary objective of optical devices in non-lethal applications is to elicit a temporary response through the targeted individual's visual system. While low-level exposures are useful for providing a warning response, systems that produce high-level exposures that may degrade visual function temporarily are increasingly sought after for tactical advantages. While systems utilizing either broadband optical radiation or laser sources are feasible for this use, functional application of both technologies and quantifying the potential degradation are key steps in the weapons development process. The degradation effects require high-fidelity assessments of exposures on human vision. To meet this need, the Air Force Research Laboratory, 711th Human Performance Wing, Human Effectiveness Directorate, Bioeffects Division, Optical Radiation Bioeffects Branch (711 HPW/RHDO) previously developed a computational model to estimate the transient visual effects created by exposure to high-intensity light sources.[1]

The current model was an evolution of a conceptual model derived largely from research on the human visual response to high-intensity monochromatic laser light sources conducted in 711 HPW/RHDO over the previous decades.[2,3] Those data, along with empirical models accepted in the scientific community for determining intra-ocular light scatter and contrast sensitivity, resulted in a first-order model of glare and photostress recovery. The original model was image-based and took a radiometric-referenced image of the optical source (an extended source) and processed it through a two-dimensional intra-ocular scatter model to calculate the light distribution on the retina, superimposed this distribution on the visual task, and estimated the glare effect induced by the reduction in target contrast.

For flash recovery, a flashblindness model was used to calculate the resultant transient relative scotoma at any given time after the exposure; this scotoma was superimposed on the visual task to estimate the reduction in the observed target contrast. For both glare and flash recovery, the visual task was of uniform luminance contrast, and obscuration levels were calculated by comparing the image contrast with a contrast threshold estimate, the contrast threshold being based upon the size of the visual task (angular subtense) and the ambient luminance.[1] Obscuration was represented visually via a binary illustration of the portions of the task in the scene that were visible, and calculated as a percentage of the target obscured. Using this approach, predictions of relative effectiveness for candidate non-lethal flashbang devices were performed as part of the improved flashbang grenade program.[4,5]

Recently, the vision model was enhanced with the inclusion of an approach that replicates the spatial frequency processing mechanisms that are found in the human visual cortex.[6] The model, called PREMO (for Photostress REcovery MOdel), approximates cortical processing by taking a complex two-dimensional visual scene and decomposing it into six spatial frequency channels.[7,8] This bandpass-filtered approach is founded on prior research published in the vision science literature for target detection and identification.[7,9] In PREMO, visual recovery following a flash exposure is estimated by modeling recovery for each spatial frequency channel, and reconstructing the visual scene at different times after the flash by recombining results from the recovering channels. The advantage of this approach over the prior model is that it does not compress the visual world into a single size and contrast; rather it represents the visual task in all its complexity, comprised of a multitude of target "sizes", contrasts, and luminance levels.

Image-based sources and visual tasks supported by PREMO allow the user flexibility in analyzing a wide variety of exposure conditions and sources. For the source, digital images from searchlights, LED arrays, thermobaric devices, and other sources can be used. Because PREMO applies digital imagery as the visual task, tasks are no longer limited to simple uniform geometric shapes: virtually any grayscale digital image can be used. In addition, the results are presented as a probability of identification at any given time after exposure. The model also has a visualization window that renders how the visual image is obscured by the optical exposure and how vision recovers after the exposure has been terminated. These features provide the capability of the model to cover a wide range of operational scenarios and allow the user to envisage the consequences of optical radiation visual effects.

1.2 Purpose and Scope

The purpose of this report is to document the mathematical basis of the Photostress Recovery Model (PREMO) and to describe its logic, function, and scope. This report describes the model algorithms in detail and their scientific underpinnings. Brief appendices provide additional details on the use of the model including the software architecture and preprocessing of the optical radiation sources.

2. MODEL DESCRIPTION

2.1 Overview

PREMO is a computational model that predicts the impact of broadband and monochromatic optical radiation on visual function. The model accepts images of the optical source and the visual task to analyze the glare and photostress recovery effects (Figure 1). In practical terms the model analyzes how visible light from intense optical sources affects the visibility of objects in a viewed scene and the time course of image detection recovery after the obstructive optical source has been removed.

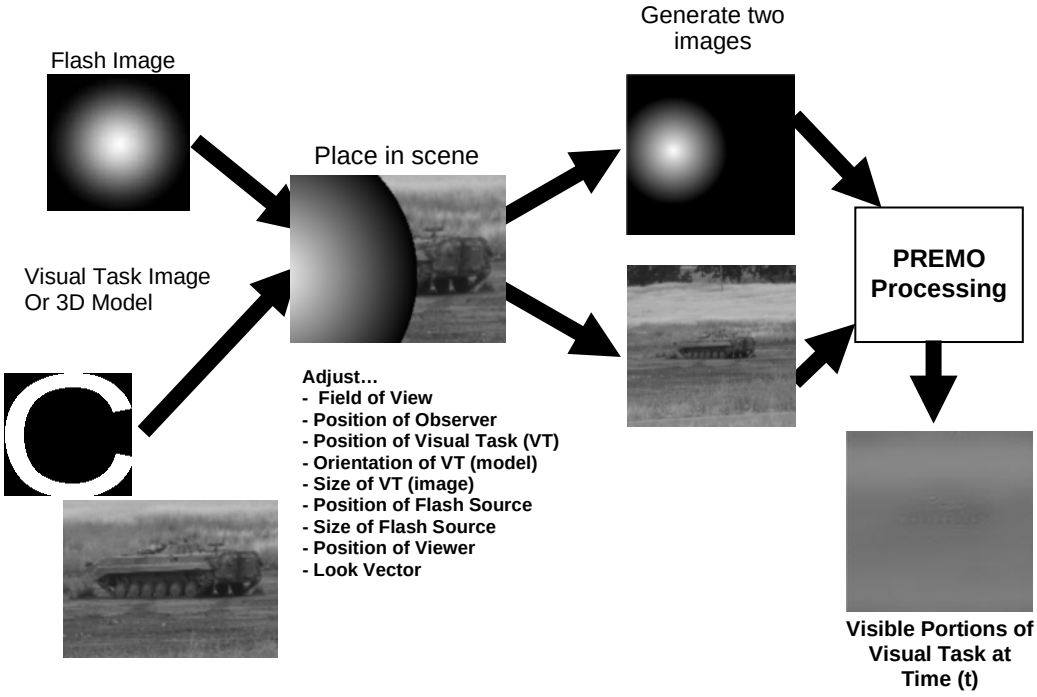

Figure 1. An illustration of how the model combines the images of the optical source and the visual task to analyze the glare and photostress recovery effects

A description of the logical steps taken by the model follows:

- A scene generator is used to transform the physical locations of the optical source, observer, line of sight, and visual task into a two-dimensional scene from the observer's point of view.

- The model input parameters include the source parameters, the source image, the mission scenario, complex scene parameters, a three dimensional object or an image of the complex scene, observer parameters, and the field of view. For an extended source the input parameters include the size, duration, measured target/object illuminance, and range at which illuminance was measured. For a laser source the input parameters include the wavelength, beam waist, range to observer, aperture waist, divergence, and laser power.

- For the complex scene, an image of the scene is used as input and the user specifies the image size and the luminance range for the scene.

- The glare and photostress recovery algorithms process the source input parameters to develop a retinal luminance image distribution. The retinal luminance image distribution can be produced using a geometric optics approach (recommended for extended sources) or convolution of the corneal luminance with the point spread function (PSF) for the human eye. The resulting distribution is processed through the spatial frequency algorithm.

- For the scene image the model generates band-pass luminance distribution matrices and low-pass luminance distribution matrices. For each band-pass luminance distribution matrix of the scene, the spatial frequency algorithm computes a reduced-contrast matrix and compares it to a detection threshold to determine recovery.

- The photostress recovery model determines recovery of the scene at the time steps provided by the user.

- Given the recovered scene at a given point in time, the probability of identification/recognition algorithm provides the probability of identifying/recognizing a target based on the recovered spatial frequency content and the extent of detectable edges.

A detailed description of the mathematical formulations and the scientific underpinnings of the model are presented in the following sections.

2.2 Components

2.2.1 Scene generation.

The OpenSceneGraph[†] 3D viewer allows the user to position one or more optical sources, the observer, and the visual task in 3D space. In order to create an accurate representation of the observer's field of view, a 3D virtual representation of the scenario is used to generate input images that can be passed and processed by the model. This is illustrated in Figure 3. This 3D virtual representation of the scene requires these parameters:

Source Image. This image file is a square, gray-scale image that represents the spatial distribution of the optical source. It is typically created as a two-dimensional circular Gaussian gradient with white at the center and black on the edges. In the figure the optical source is represented by a thermobaric device (flashbang).[‡]

Visual Task Image. This image file represents the visual task in the scene that is to be obscured. A 3D model file (e.g. a 3D model of a soldier created in 3D Studio Max, as in

[†] See Appendix A for a description of the OpenSceneGraph software architecture and the type of files it supports.

[‡] In the absence of a user-supplied source image, a simulated source image can be generated by the model (a Gaussian or a flat top distribution are currently available).

the figure) or a 2D image may be used to represent the visual task in the 3D scene. The vision model requires luminance values for each pixel in the complex scene. In its current configuration, the PREMO accepts maximum and minimum luminance values as user inputs, and uses these together with the image greyscale values to scale the luminance of each pixel within the complex scene.

Scenario Geometry. The scenario geometry dictates the positioning of all of the elements in the scene and includes

a) Visual task position, orientation, and scale,

b) Source image position, orientation, and scale,

c) Observer position, orientation, and field of view. The observer is shown as a schematized camera (in yellow) in the figure. The scene from the observer's point of view is shown in Figure 3.

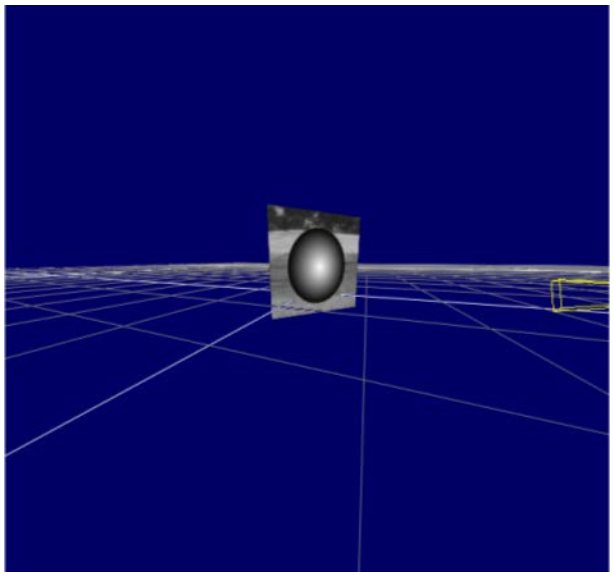

Figure 2. A visual representation of the scenario in 3D space

Figure 3. Images of the visual task and the flash source as seen by the observer in the scene

The geometric relationships between the objects in the scenario determine the visual effect of the source. The observer, source(s), and visual task can each be independently placed anywhere in the scene. In most situations the source needs to be in the vicinity of the line of sight to have any significant effect. The underlining infrastructure supports a different point of fixation for each time step to simulate eye movements, but typically only one or two points of fixation are used for the entire simulation.

2.2.2 Optical source processing.

This component calculates the optical source fluence at the cornea for the viewing distance and propagates the source through the optical media of the eye to create an image on the retina.

2.2.2.1 Corneal light distribution.

For a broadband source, light from the source[§] is propagated to the eye to obtain the corneal light distribution. The quantity source can either be a single value (for a point source such as a laser) or an array, as in an image (for an extended source). To calculate the corneal light distribution for an extended source, the model uses an image of the source and its illuminance, *E(D)*, which is an input value to the model. If the illuminance was originally measured at a given distance, *D*, the inverse square law is used to evaluate the illuminance, *E(R)*, at the observer distance, *R*:

$$E(R) = E(D) \cdot \left(\frac{D}{R} \right)^2 . \tag{1}$$

This computed illuminance is then used with the source image to define the corneal illuminance distribution. For each pixel in the source image the corneal illuminance, $E(x_i,y_j)$, (for glare) and the integrated illuminance, $H(x_i,y_j)$, (for photostress recovery) are given by the following equations:

$$E(x_i, y_j) = \frac{E(R) \cdot g(x_i, y_j)}{\sum_{i,j} g(x_i, y_j)} \tag{2}$$

$$H(x_i, y_j) = \frac{t \cdot E(R) \cdot g(x_i, y_j)}{\sum_{i,j} g(x_i, y_j)} \ , \tag{3}$$

where $g(x_i, y_i)$ is the gray-scale value of a pixel in the source image.

For a laser source, the model calculates the corneal light distribution from the laser parameters supplied by the user; wavelength, divergence, beam waist, range to the observer, beam profile, and distribution (Gaussian or flat top). Given the laser parameters, the beam diameter at the observer location is given by the following equation:

[§] The specifications of the optical source, including the required input parameters, source image, and conversion to photometric units are detailed in Appendix B for both laser and broadband sources.

$$D_L = \sqrt{a^2 + (r - r_o)^2 \phi^2} \,. \tag{4}$$

The parameter a is the beam waist, r is the range to observer, r_o is the aperture waist, and ϕ is the beam divergence.

The laser power transmitted by an aperture diameter, D_f, is given by:

$$\Phi = \Phi_o \left[1 - e^{-\left(\frac{D_f^2}{D_L^2} \right)} \right]. \tag{5}$$

The parameter Φ_o is the laser output power. For a circular beam, the irradiance at the cornea is given by:

$$E = \frac{\Phi}{\pi \left(\frac{D_L}{2} \right)^2} = \frac{1.27\Phi}{D_L^2} \,. \tag{6}$$

The Illuminance E_v is related to the spectral irradiance E_λ by the following equation

$$E_v = 683 \cdot \int E_\lambda \cdot V_\lambda \cdot d\lambda \,, \tag{7}$$

where V_λ is the photopic luminous efficiency function.

2.2.2.2 Intraocular light scatter.

Light from a point source is not focused perfectly on the retina, but instead it is scattered within the eye, which produces a veiling luminance over the field of view. The scattered light causes a reduction in image contrast, particularly for objects in the field of view close to the source. The masking effect caused by the light scattered in the ocular media is termed veiling glare. To evaluate the effects of veiling glare, an algorithm for intraocular scatter is used to model the distribution of a light source on the retina. The function used to predict the distribution of the light scattered based on the light distribution at the cornea is referred to as the point spread function (PSF).[10-13]

An analytical expression for the PSF that closely fits experimental data was developed by Vos.[13] The Vos formulation distinguishes the different components of entoptic light scatter (anterior segment, scleral wall, and epithelium) and includes the dependency of the PSF on age (A) and eye pigmentation (P). The current model uses this expression to compute the image profile of a point source on the retina:

$$PSF(\theta) = Anterior(\theta) + Wall(\theta) + Epithelium(\theta) \ , \tag{8}$$

where:

$$Anterior(\theta) = 1.03 \times \left(1 - 0.1\left(\frac{A}{70}\right)^4\right)\left(\left(\frac{8.83\times10^6}{\left(1+\left(\frac{\theta}{0.0046}\right)^2\right)^{1.5}}\right) + \left(\frac{1.43\times10^5}{\left(1+\left(\frac{\theta}{0.045}\right)^2\right)^{1.5}}\right)\right) + 0.46\left(1+1.85\left(\frac{A}{70}\right)^4\right)\left(\left(\frac{10^3}{1+\left(\frac{\theta}{0.1}\right)^2}\right) + 7\times10^{-8}\theta^2\right) \ , \tag{9}$$

$$Wall(\theta) = 3.5\times10^{-5}\left(\frac{(105-\theta)}{\cos(0.92(\theta-5))}\right) \ , \tag{10}$$

$$Epithelium(\theta) = 0.175P\left(\left(\frac{16}{(\theta+0.1)^3}\right) + \left(\frac{1}{\theta+0.1}\right)\right) \ , \tag{11}$$

and θ is eccentricity from the center of the source on the retina in degrees.

Figure 4 shows the shape of the PSF, which describes the magnitude of the intraocular scatter as a function of the angle between the incoming source and the retinal location. The intensity is greatest for the central, zero-degrees location, and falls off as the angle increases. For an extended source the same scattering profile is used, but it is convolved with a two-dimensional light distribution rather than a point source.

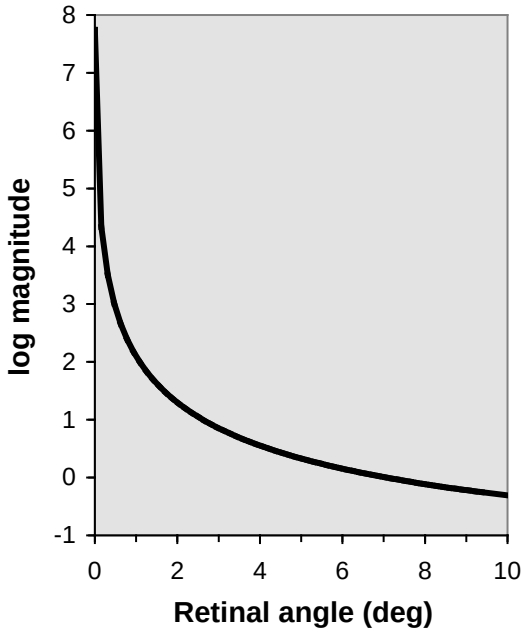

Figure 4. The intensity profile of a point light source as a function of retinal angle due to optical scatter within the eye

The model convolves the input corneal light distribution, $E(x, y)$, with the intraocular point spread function, $PSF(\theta)$. The output of the algorithm is a retinal image luminance profile:

$$L(x, y) = E(x, y) \otimes PSF(\theta), \tag{12}$$

where $L(x,y)$ is the retinal luminance distribution in cd·m^{-2}, which represents the source glare field.

2.2.2.3 Geometrical optics approximation.

For an extended source, light from the flash is collected by the eye and the flash image is focused onto the retina. A schematic diagram is shown in Figure 5.

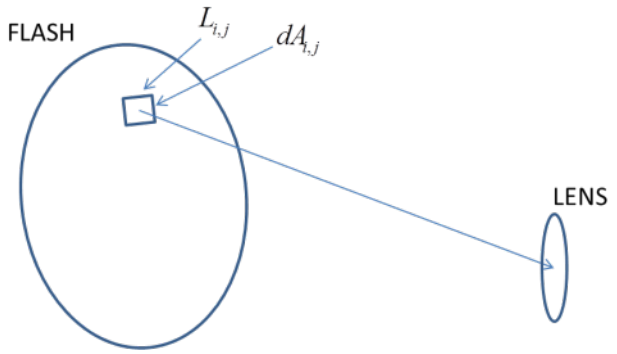

Figure 5. Light collected by the lens and focused by the eye

Light with luminance, $L_{i,j}$ is emitted from an element in the flash with area $dA_{i,j}$. The distance from the element to the eye is $R_{i,j}$. Across all the elements in the flash, the average luminance of the flash, L, for N elements is given by:

$$L = \frac{1}{N} \sum_{i,j} L_{i.j} \quad . \tag{13}$$

For an image of the flash, in terms of gray scale $g_{i,j}$, the average gray scale value, g, is given by:

$$g = \frac{1}{N} \sum_{i,j} g_{i.j} \quad , \tag{14}$$

and the luminance of each element is:

$$L_{i.j} = L \frac{g_{i.j}}{g} \quad . \tag{15}$$

For each elemental area, $dA_{i,j}$, the illuminance, $E_{i,j}$, at the eye is calculated from the source measurements scaled for the viewing distance by the inverse square law:

$$E_{i.j} = L_{i.j} \frac{dA_{i.j}}{R_{i,j}^2} \quad . \tag{16}$$

The total illuminance at the eye, *E*, is known from sum of the individual elements,

$$E = \sum_{i,j} E_{i.j} \quad . \tag{17}$$

Assuming that all elements have the same elemental area, *dA*, and are located a distance *R* from the lens, the total illuminance is given by

$$E = \frac{dA}{R^2} \sum_{i,j} L_{i.j} = \frac{N\ dA}{R^2} L = \frac{A}{R^2} L \quad . \tag{18}$$

Knowing the area of the flash, *A*, and the distance from the observer, *R*, the retinal luminance of each element, $L_{i,j}$, is given by

$$L_{i.j} = \frac{R^2}{A} E(R) \frac{g_{i,j}}{g} = \frac{D^2}{A} E(D) \frac{g_{i,j}}{g} \, . \tag{19}$$

2.2.3 Spatial frequency hierarchy.

Psychological studies have demonstrated the existence of a frequency selective mechanism in the human visual system. Previously, a number of models have been developed to simulate the human vision system response using a set of cortex filters.[7,14]. Our current cortex filters modeling is based on a model originally developed by Watson[14], as improved by Daly.[15] As defined by both Watson and Daly, the cortex filters are modeled by two classes of filters, for radial frequency selectivity and for orientation selectivity. Our current implementation accounts for the radial frequency selectivity, but not the orientation selectivity. The cortex filters are formed as differences of a series of two-dimensional mesa filters characterized by a flat pass-band, a transition region, and a flat stop-band region. This ensures that the filter set sums to unity. The transition region is modeled with a Hanning window, so that the mesa filter can be completely described by its half-amplitude frequency, $\rho_{1/2,}$ and a transition width, *tw*, as follows:

$$mesa\ (\rho) = \begin{cases} 1.0 & for\ \rho < \rho_{1/2} - \dfrac{tw}{2} \\ \dfrac{1}{2}\left(1 + \cos\left(\dfrac{\pi(\rho - \rho_{1/2} + tw/2)}{tw}\right)\right) & for\ \rho_{1/2} - \dfrac{tw}{2} < \rho < \rho_{1/2} + \dfrac{tw}{2} \\ 0.0 & for\ \rho > \rho_{1/2} + \dfrac{tw}{2} \end{cases} \tag{20}$$

where each cortex filter is characterized by a flat pass-band and a transition region. The cortex filter is formed by the difference of two mesa filters evaluated with different half-amplitude frequencies. The k^{th} cortex filter is given by:

$$cortex_k(\rho) = \begin{cases} mesa(\rho)\big|_{\rho_{1/2}(k-1)} - mesa(\rho)\big|_{\rho_{1/2}(k)} & for\ k = 1, K-2 \\ mesa(\rho)\big|_{\rho_{1/2}(k-1)} - base(\rho)\big|_{\rho_{1/2}(k)} & for\ k = K-1 \end{cases}, \quad (21)$$

where the total number of filters is K and the half-amplitude frequency for a mesa filter, $\rho_{1/2}(k)$, is given by:

$$\rho_{1/2}(k) = 2^{k}. \quad (22)$$

The lowest-frequency filter, *base(ρ)*, referred to in this document as a low-pass filter, is modeled by a truncated Gaussian function, given by:

$$base(\rho) = \begin{cases} e^{-(\rho^2/2\sigma^2)} & for\ \rho < \rho_{1/2} + \dfrac{tw}{2} \\ 0 & for\ \rho \geq \rho_{1/2} + \dfrac{tw}{2} \end{cases}, \quad (23)$$

where σ is defined as:

$$\sigma = \frac{1}{3}(\rho_{1/2} + \frac{tw}{2}), \quad (24)$$

and $\rho_{1/2} = 2^{-K}$.

In the current implementation, the transition width, *tw*, of each filter is a function of its defined half-amplitude frequency as follows:

$$\text{tw} = \tfrac{2}{3}\,\rho_{1/2}. \quad (25)$$

The resulting filter set is shown in Figure 6.

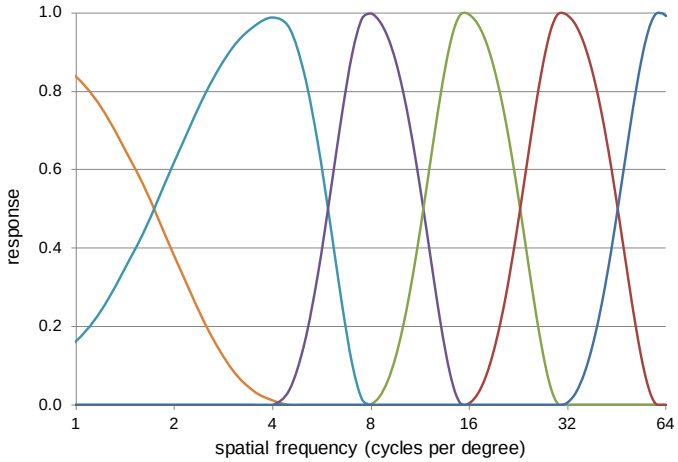

Figure 6. The cortex filter series

2.2.4 Glare and photostress recovery.

PREMO predicts two effects of high-intensity light sources: veiling glare and photostress recovery. Glare is defined as the masking effect of a bright light caused by light scattered in the ocular media which produces a veiling luminance over the field of view. Photostress is a psychophysical process which persists after a bright light exposure. This effect is because photostress induces an afterimage in the form of a transient scotoma that subsequently recedes; the effect is temporary and visual sensitivity eventually returns to normal and normal vision is restored. Photostress recovery time (PSRT) is the time between when the light is removed and when the observer can see a particular visual stimulus. In the study of both glare and photostress recovery, the effect is measured by comparison to a physical light source that produces the same visual effect; this has given rise to the generally accepted metric as the equivalent veiling or equivalent background luminance (EBL).[11] In addition, both glare and photostress recovery effects depend not only on the parameters of the inducing light source, but also on the properties of the visual task and the visual scene. The size and brightness of the visual task, the ambient illumination level, and visual task contrast threshold all play a critical role in determining the extent of glare and the time course of photostress recovery.

2.2.4.1 Contrast threshold estimation.

Contrast is the difference in luminance and/or color that makes an object distinguishable. In visual perception, contrast is determined by the difference in the color and luminance of the object and other objects within the same field of view. The model uses luminance contrast detection as the critical visual function. Luminance contrast detection is the ability to perceive the presence of two objects to a difference in luminance between the two. Luminance contrast threshold and its measurement have been extensively studied in the vision science literature and are well understood.[16,17] Luminance contrast detection is also consistent with the analysis of optical radiation visual effects because the effect of an intense light source is to reduce the luminance contrast of objects and therefore reduce a subject observer's visibility.

The contrast sensitivity function (CSF) of the human eye developed by Barten[18] is used in PREMO to calculate contrast thresholds based on the scene parameters (contrast threshold is simply the inverse of the CSF). The CSF gives the contrast sensitivity as a function of spatial frequency. Figure 7 shows a family of contrast threshold curves calculated for a field of view size of 10° × 10° and various visual task luminance levels. As shown in Figure 7, the contrast threshold reaches its minimum between 1 and 10 cycles per degree. For a standard observer the CSF is given by Equation (26) below.

$$CSF(f) = \frac{5200\, e^{-0.0016 \times f^2 (1+100/L)}}{\sqrt{(1+\frac{144}{\chi_0^2}+0.64\times f^2)(\frac{63}{L^{0.83}}+\frac{1}{1-e^{-0.02\times f^2}})}} \tag{26}$$

In this equation f is the spatial frequency in cycles/degree, L is the luminance in cd·m^{-2}, and χ_0^2 is the angular object area in square degrees. The constant 5200 in the numerator is valid for binocular viewing. For monocular viewing, it is a factor $\sqrt{2}$ smaller, or 3700.

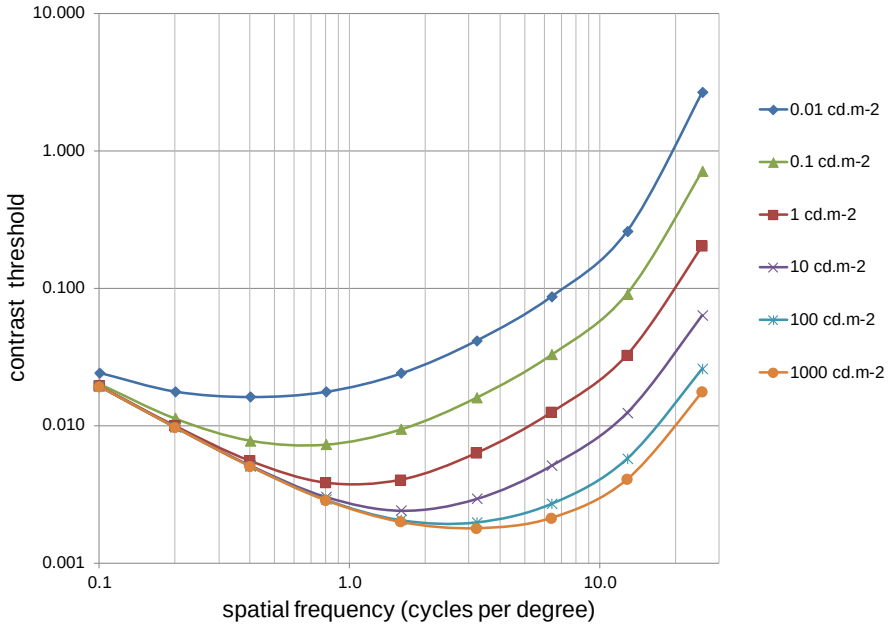

Figure 7. Contrast threshold calculated using Barten's formula for a field size of 10° × 10°

2.2.4.2 Processing glare effects.

As described earlier, the model uses the visual task image grayscale levels and user inputs for the maximum and minimum luminance to calculate luminance values across the visual scene. This step renders the image of the scene into units appropriate for it to be added to the glare retinal image distribution. The superposition of glare on the visual task is accomplished by adding the glare retinal image luminance distribution, defined by Equation (12), or, for an extended source, by Equation (19), to the visual task image luminance. The combined image is known as the EBL reduced visual task image $ERVT(x, y)$ and it is given by:

$$ERVT(x, y) = EBL(x, y) + VT(x, y), \tag{27}$$

where $EBL_{(x,y)}$ is the retinal image distribution of the glare, and $VT_{(x,y)}$ is the visual task image luminance. $ERVT_{(x,y)}$ is convolved with each of the six cortex filters described above to produce a set of five band-pass filtered images denoted by $ak_{(x,y)}$, and a low-pass image $ao_{(x,y)}$. Each band-pass filtered image, $ak_{(x,y)}$, is obtained using Equation (28):

$$a_k(x, y) = ERVT(x, y) * g_k(x, y), \tag{28}$$

where the array $g_k(x,y)$ represents the inverse Fourier Transform of the cortex filter, $cortex_k(\rho)$, and $*$ is the convolution operator.

The low-pass image, $a_o(x,y)$, is generated by convolving the ERVT image with the lowest-frequency filter $base(\rho)$,

$$a_0(x, y) = ERVT(x, y) * base(x, y), \tag{29}$$

where *base(x,y)* is the inverse Fourier Transform of the cortex filter *base(ρ)*. For each band-pass filtered image we define a corresponding local luminance mean image, *l(x,y)*, which is a low-pass filtered version of the image containing all the energy below the band:

$$l_i(x,y) = a_0(x,y) + \sum_{k=1}^{i-1} a_k(x,y) \quad . \tag{30}$$

A two dimensional local contrast array, $C_i(x,y)$, is also defined for each band-pass filtered image. Contrast is computed as the ratio of band-pass filtered image to the corresponding low-pass filtered image:

$$C_i(x,y) = \frac{a_i(x,y)}{l_i(x,y)} \quad , \tag{31}$$

where $l_i(x,y) > 0$.

This definition provides a local contrast measure for every band that depends on the local energy at that band and the local background luminance. The contrast at each pixel is compared to the corresponding contrast threshold. The model transforms below-threshold pixels to average luminance to show which part of the band-pass filtered image is being obscured by the glare source. The recovered scene is computed by adding the five band-pass filtered images each five-threshold transformed and the low-pass image $a_0(x,y)$.

2.2.4.3 Processing photostress recovery effects.

The photostress recovery analysis describes the recovery of visual sensitivity after the source has been turned off though a visual process known as dark adaptation. As with the glare model, the photostress recovery model also uses the equivalent background principal to model the recovery in sensitivity. The effects of the source are again represented as a veil of light, but the effect fades with time. The initial step in calculation involves expressing the flash exposure in terms of the integrated retinal illuminance. For this, by analogy to the glare model, the PSF is applied to the flash energy to estimate the retinal distribution of the flash, but calculated as an integrated luminance in $cd \cdot m^{-2} \cdot s$; the product of the equivalent background luminance and the exposure duration. Then the integrated luminance is expressed in terms of integrated retinal illuminance, *RI*, in photopic troland-seconds (td·s) by multiplying by the area of the pupil:

$$RI(x,y) = L(x,y) \cdot t \cdot PA \,, \tag{32}$$

where $L(x,y)$ is the retinal luminance distribution in $cd \cdot m^{-2}$, *PA* is the pupil area in mm^2, and *t* is the exposure duration in seconds. *RI(x,y)* is the resultant integrated retinal illuminance distribution for the exposure. The photostress recovery analysis uses the integrated retinal illuminance from the photostress stimulus to model the recovery of visual sensitivity over time.[19] Recovery is represented as an equivalent background luminance distribution that decays with time according to a power function, *EBL(x,y,t)*.[20] For the recovery function, the integrated retinal illuminance distribution is first converted to a "flash energy" distribution, *F(x,y)*, by taking its logarithm:

$$F(x,y) \;=\; \log_{10}\left[RI(x,y)\right]. \tag{33}$$

These values are then used as input into the decay function, and at any time after exposure, the *EBL(x, y, t)* of a pixel in the retinal illuminance distribution is given by:

$$EBL(x,y,t) = 10^{m\cdot Log_{10}(t)\,+\,c}, \tag{34}$$

where *m* and *c* are functions of the flash energy and are given by:

$$m = \begin{cases} 1.01F - 8.919 & for\ F < 6.11\ \log \text{td}\cdot\text{s} \\ -2.73224 & for\ F \geq 6.11\ \log \text{td}\cdot\text{s} \end{cases} \tag{35}$$

$$c = -0.4066\cdot F^{2} + 6.4012\cdot F - 19.427\,. \tag{36}$$

Note that the decay function takes two different forms, one for exposure energy values less than 6.11 log td·s, and another for values greater than this.

The behavior of the function is shown in Figure 8, which shows the decay of the EBL with time for different energies in the initial flash exposure.

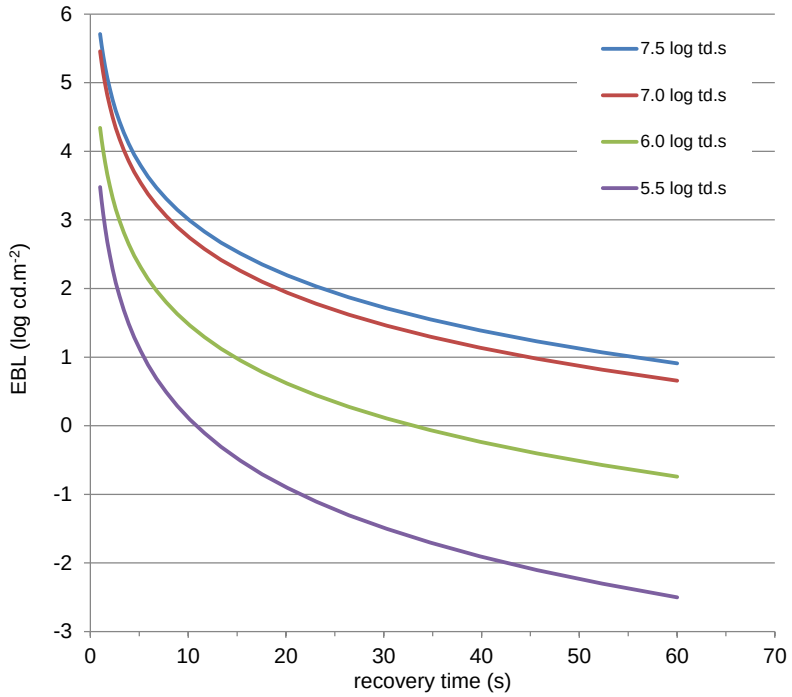

Figure 8. The decay of the EBL after the exposure is terminated

Recovery of visual function is processed differently compared to the glare analysis. This is because the persistent effect of the flash varies with time after the initial exposure. For the glare the EBL is used as a static contrast-reducing mechanism, whereas for photostress recovery the effect of the EBL at time *t* must be evaluated as time after the exposure progresses.

For the recovery analysis, the visual task image, *VT(x,y)*, in cd·m^{-2} is convolved with each of the six cortex filters described previously to produce a set of five band-pass filtered images denoted by $a_k(x,y)$ and a low-pass image $a_0(x,y)$. The band-pass filtered image $a_k(x,y,)$, resulting from the convolution is written as:

$$a_k(x,y) = VT(x,y) * g_k(x,y), \tag{37}$$

where the array $g_k(x,y)$ represents the inverse Fourier Transform of the cortex filter, $cortex_k(\rho)$, and * is the convolution operator. The low-pass image $a_0(x,y)$ is generated by convolving the visual task image with the lowest-frequency *filter base(ρ)*:

$$a_0(x,y) = VT(x,y) * base(x,y) \tag{38}$$

where *base(x,y)* is the inverse Fourier Transform of the cortex filter *base(ρ)*.

For each band-pass filtered image a two-dimensional contrast array $C_i(x,y,t)$ is defined. For each band-pass filtered visual task image and for the low-pass visual task image, the contrast is given by Equation (38).

$$C_i(x,y,t) = \frac{a_i(x,y)}{LPVT_i(x,y) + EBL(x,y,t)} \qquad i = 0, 1, 2, 3, 4, \text{and } 5, \tag{39}$$

where, $LVPT_i(x,y)$ and $EBL(x,y,t)$ denote the low-pass visual task luminance and the EBL at time *t*, respectively.

The low-pass visual task luminance ($LVPT_i(x,y)$) for a given visual task band-pass image is defined as the visual task image containing all energy below that spatial frequency band.

$$LPVT_i(x,y) = \begin{cases} a_0(x,y) + \sum_{k=1}^{i-1} a_k(x,y) & i = 2,3,4,5 \\ a_0(x,y) & i = 1 \end{cases} \tag{40}$$

The contrast at each pixel is compared to the corresponding contrast threshold. The model transforms below-threshold pixels to average luminance to show which part of the band-pass filtered image is not visible. The recovered scene is computed by adding the six band-pass filtered images with individual thresholds. The model can process photostress recovery over a period of time to show a time-elapsed sequence of recovery. Figure 9 illustrates this process.

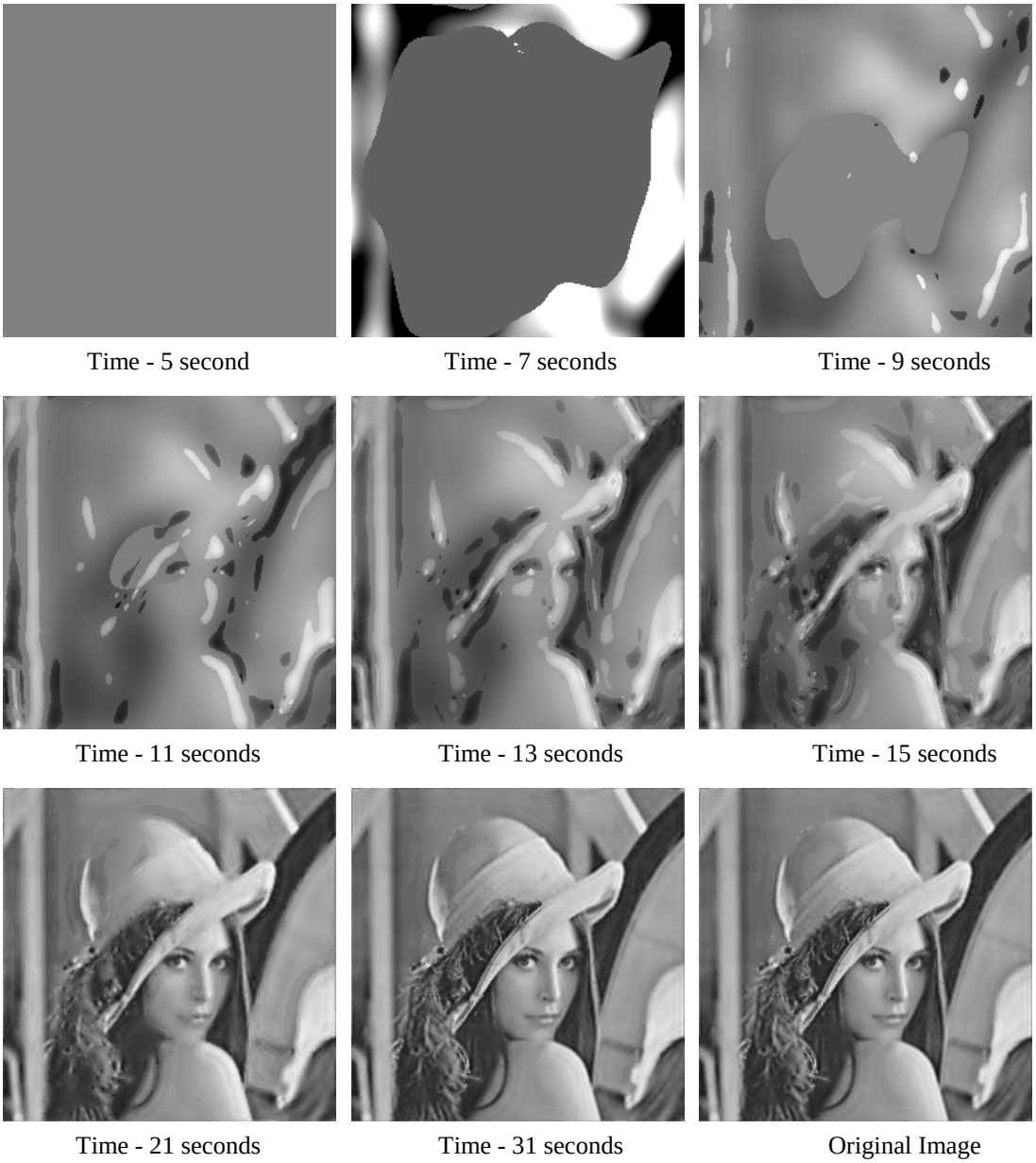

Figure 9. An illustration of how recovery of visual sensitivity after exposure to a bright light flash is represented in the model

Using the example illustrated in Figure 9, careful inspection of the recovery images reveals a systematic recovery process that starts with low spatial frequencies and progresses through to the high frequencies with time. The scene appeared to have fully recovered to include most of the high spatial frequency content (fine details) after 31 seconds. This exemplifies how the recovery time for a given visual task in a given scene will be highly dependent on the spatial frequency content of the scene. Using the same input parameters, Figure 10 shows the recovery images for each of the spatial frequency bands.

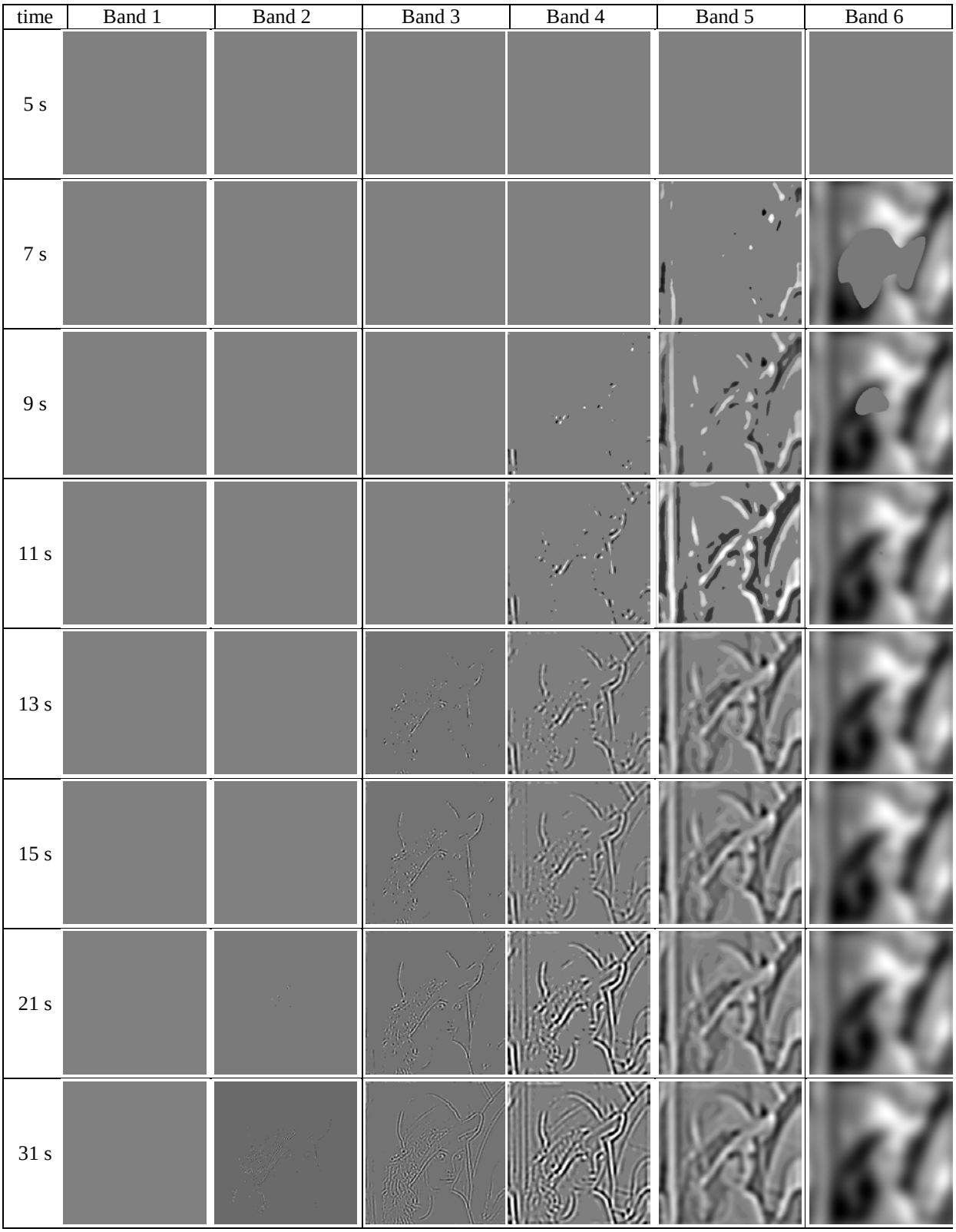

Figure 10. An illustration of the recovery process for each frequency band

2.2.4.4 Visibility metric.

Developing a visibility metric for arbitrary task located in an arbitrary scene is a very challenging task. This is due to the recovery dependence on the spatial frequency content of the scene. An initial approach was taken for the model that involved assigning a visibility weight for each filtered band and assigning a contribution share as a fraction for each band. The obscuration level at a given post-exposure time was determined from the number of pixels recovered, the weight assigned to the frequency band, and the value of the contribution share.

2.2.5 Probability of identification/recognition.

The Visual Effects model provides two approaches to predict the probability of identifying a target in the scene at any given post-exposure time: the empirical Target Transform Probability Function (TTPF) approach developed by Johnson and Lawson[21], and the Contrast Based Edge Detection approach based on the work of Johnson.[22]

2.2.5.1 Target transform probability function (TTPF).

The TTPF relates the probability of performing a task to the ratio of the number of cycles one can resolve across the minimum dimension of a target to the standard number given in the Johnson Criteria.[23] Therefore, given the level of resolvable spatial frequency on the target (N) and the recommended spatial frequency level for 50% probability to detect, identify, or recognize a target (N_{50}), the probability can be predicted based upon the following empirically derived formulation:

$$P_t = \frac{\left(N/N_{50}\right)^E}{1+\left(N/N_{50}\right)^E}, \tag{41}$$

where

$$E = 2.7 + 0.7 \times \left(\frac{N}{N_{50}}\right). \tag{42}$$

2.2.5.1 Contrast based edge detection approach.

The formulation of an edge detection algorithm to respond to contrast rather than absolute luminance values provides a consistent ground for edge detection in a scene with irregular visible spectrum distribution. Given the luminance distribution of the scene, the contrast based Sobel operator is given by the following formula:

$$S_{ij} = \frac{\left|N_{ij} \otimes A_3\right| + \left|N_{ij} \otimes B_3\right|}{\left|N_{ij} \otimes C_3\right| + d}. \tag{43}$$

where N_{ij} is the numerical luminance value of the row j, column i element of the matrix that represent the scene. The symbol $\otimes$ represents the convolution operator, while the convolution masks denoted by A_3 and B_3 are given by:

$$A_3 = \begin{pmatrix} -1 & -2 & -1 \\ 0 & 0 & 0 \\ 1 & 2 & 1 \end{pmatrix} \qquad B_3 = \begin{pmatrix} -1 & 0 & 1 \\ -2 & 0 & 2 \\ -1 & 0 & 1 \end{pmatrix}, \tag{44}$$

and the averaging mask C_3 is given by:

$$C_3 = \begin{pmatrix} 1 & 1 & 1 \\ 1 & 1 & 1 \\ 1 & 1 & 1 \end{pmatrix}. \tag{45}$$

The value of d is to be chosen to provide an acceptable trade-off between noise sensitivity and the dynamic range for the combination of the human visual system and scene. In the current implementation the value of d is set to unity, but a threshold formula (S_{th}) for the contrast-based Sobel operator as a function of contrast (C) was developed for scene luminance ranges from 2 to 180 cd·m^{-2} (Equation 46 and Figure 11). Further work is needed to extend this function and define thresholds for very bright and very dim conditions.

$$S_{th} = 1.5222 \cdot C^4 - 3.9496 \cdot C^3 + 2.9591 \cdot C^2 - 0.1565 \cdot C + 0.317 \tag{46}$$

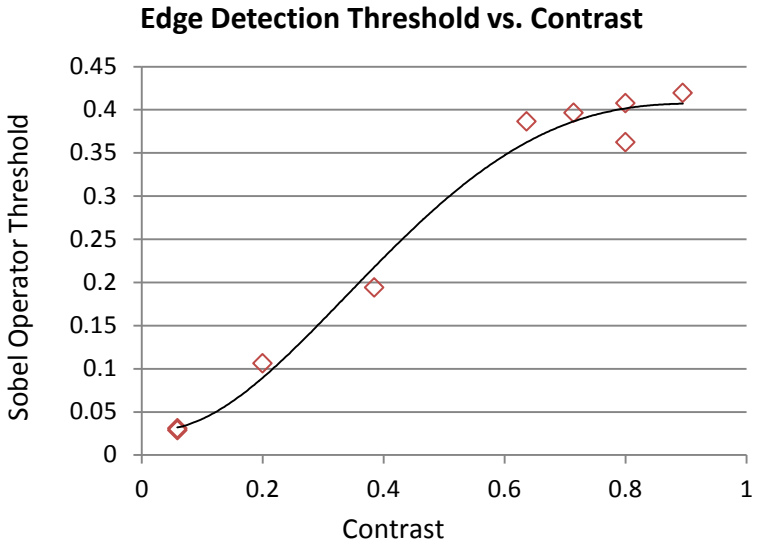

Figure 11. Sobel operator threshold as a function of contrast

The probability of finding a task in a scene at a given post-exposure time can be predicted using the cumulative normal distribution, *cdf* (Equation 47), given that the fraction of recovered edges, μ, which produces recognition in 50% of the trials is established:

$$cdf = \int_{-\infty}^{x} \frac{1}{\sqrt{2\pi\sigma^2}} e^{\frac{-(t-\mu)^2}{2\sigma^2}} dt = \frac{1}{2}\left[1 + erf\left(\frac{x-\mu}{\sigma\sqrt{2}}\right)\right] \quad (47)$$

3. APPLICATIONS

This experimental approach and computational analysis model can be used for a variety of applications such as aviation warning systems, military operations, and law enforcement where intentional optical exposures are used as a non-lethal deterrent. For example, visual effectiveness of non-lethal dazzlers,[24-26] thermobaric devices,[5] and laser countermeasures in military operations have been assessed with the more simplistic predecessor of this model.[27,28] The model may also be used to evaluate risks to safety and job performance in situations where intense optical sources are employed.

4. SUMMARY

The Photostress Recovery Model (PREMO) is a computational model of the glare and photostress recovery effects of optical radiation. The main parts of the model are a scene generation component, an optical source processing component, a spatial frequency processing component, a glare and photostress recovery processing component, and a probability of identification/recognition processing component. The optical-source component processes input from broadband or laser sources and propagates light from the source to the retina. A scene generation module specifies the spatial relationships between the observer, radiation source, and visual task and creates a representation of the scene from the observer's point of view. The spatial frequency processing component combined with the visual effects processing component estimates the effects of glare and photostress recovery on task visibility considering the spatial frequency content of the scene. The probability of identification/recognition processing provides an estimate of the probability to identify/recognize a target in the scene at a given point in time. The model output provides a quantitative analysis of visual obscuration and recovery. The model is based on an extensive literature on optics, vision science, and digital image processing.

PREMO is a useful tool to assess the extent of visual disruption for a variety of sources and operational scenarios. The current instance of the model moves beyond simple contrast detection using a single background and visual task luminance into contrast detection of a complex scene with varying luminance based on a model of the spatial frequency processing in the visual cortex. It establishes a firm foundation for future research for providing a higher-fidelity model and understanding of the temporal effects of optical radiation on the human vision system.

Separate publications that describe the validation studies that were conducted in conjunction with the development of the model have been issued.[29-31]

5. REFERENCES

1. Kosnik, W. D., Ahmed, E. M., Huantes, D. F., Early, E. A., & Pingry, R. E. (2008). Mathematical modeling of laser and broadband optical radiation visual effects. Technical Report AFRL-RH-BR-TR-2008-0045, Air Force Research Laboratory, Brooks City Base, TX 78235.

2. Menendez, A. R., & Smith, P. A. (1990). Model for predicting the effects of laser exposures and eye protection on vision. *Proc SPIE, 1207*, 21-33.

3. Kosnik, W. D., & Smith, P. A. (2003). Flashblindness and glare modeling of optical radiation. Technical Report AFRL-HE-BR-TR-2003-0069, Air Force Research Laboratory, Brooks City-Base, TX 78235.

4. Joint Non-Lethal Weapons Program. (2011, October). *Improved Flash Bang Grenade*, [Fact Sheet]. Available at: http://jnlwp.defense.gov/pdf/pressroom/IFBG%20Fact%20Sheet%20Oct%202011.pdf.

5. Early, E. A., Kosnik, W. D., Huantes, D. F., Ahmed, E. M., Zohner, J. J., Chavey, L. J., Thomas, R. J., & Notabartolo, J. V. (2006). Optical hazard and visual effects analyses of flashbang devices tested in 2004 and 2005. Technical Report AFRL-HE-BR-TR-2006-0063, Air Force Research Laboratory, Brooks City Base, TX 78235.

6. Thomas, R. J., McLin, L. N., Ahmed, E. M., Smith, P. A., Stringham, J. M., Huantes, D. F., Tessier, P., & Early, E. A. (2014). Computational modeling of the photostress recovery model (PREMO). Technical Report AFRL-RH-FS-TR-2014-xxxx, Air Force Research Laboratory, Fort Sam Houston, TX 78234.

7. Peli, E. (1990). Contrast in complex images. *Journal of the Optical Society of America A, 7*, 2032-2040.

8. Peli, E. (1997). In search of a contrast metric: matching the perceived contrast of Gabor patches at different phases and bandwidths. *Vision research, 37*, 3217-3224.

9. Peli, E. (1996). Test of a model of foveal vision by using simulations. *Journal of the Optical Society of America. A, Optics, image science, and vision, 13*, 1131-1138.

10. Toet, A., Ijspeert, J. K., Vos, J. J., & Walraven, J. (1995). Computing the retinal image profile. Report TNO-TM 1995 C-35, TNO Human Factors Institute, Soesterberg, The Netherlands.

11. Stiles, W. S., & Crawford, B. H. (1937). The effect of a glaring light source on extra-foveal vision. *Proceedings of the Royal Society*, 255-280.

12. Ijspeert, J. K., van den Berg, T. J., & Spekreijse, H. (1993). An improved mathematical description of the foveal visual point spread function with parameters for age, pupil size and pigmentation. *Vision research, 33*, 15-20.

13. Vos, J. J., & van den Berg, T. J. T. P. (1997). On the course of the disability glare function and its attribution to the components of ocular scatter. Chairman's Report CIE TC 1-18, Commission de l'Eclairage.

14. Watson, A. B. (1987). The cortex transform: rapid computation of simulated neural images. *Computer vision, graphics, and image processing, 39*, 311-327.

15. Daly, S. J. (1992). *Visible differences predictor: an algorithm for the assessment of image fidelity.* Proceedings of the SPIE/IS&T 1992 Symposium on Electronic Imaging: Science and Technology: International Society for Optics and Photonics.

16. Blackwell, H. R. (1946). Contrast thresholds of the human eye. *Journal of the Optical Society of America, 36*, 624-643.

17. Hood, D. C., & Finkelstein, M. A. (1986). Sensitivity to light. In K. R. Boff & L. Kaufman & J. P. Thomas (Eds.) *Handbook of perception and human performance. Volume 1. Sensory processes and perception* (pp. 5-1 to 5-66). New York: Wiley and Sons.

18. Barten, P. G. J. (2003). Formula for the contrast sensitivity of the human eye. *Proc SPIE, 5294*, 231.

19. Crawford, B. H. (1947). Visual adaptation in relation to brief conditioning stimuli. *Proceedings of the Royal Society of London. Series B: Biological Sciences, 134*, 283-302.

20. Smith, P. A. (1996). *A study of the transient effects of high energy laser light on visual function.* Unpublished PhD thesis, University of London, London, England.

21. Johnson, J., & Lawson, W. (1974). *Performance modeling methods and problems.* Proceedings of the Proceedings of the IRIS Imaging Systems Group.

22. Johnson, R. P. (1990). Contrast based edge detection. *Pattern Recognition, 23*, 311-318.

23. Johnson, J. B. (1958). Analysis of image forming systems, *Image Intensifier Symposium* (pp. 244-273). Ft. Belvoir, Va: U.S. Army Research and Development Laboratories

24. Early, E. A., Chavey, L. J., Rogers, B. Z., Kosnik, W. D., & Mitchell, W. E. (2006). Hazard analysis and visual effectiveness of the Vector Scientific Vectorbeam. Technical Report AFRL-HE-BR-TR-2006-0050, Air Force Research Laboratory, Brooks City Base, TX 78235.

25. Early, E. A., Chavey, L. J., Rogers, B. Z., Kosnik, W. D., & Mitchell, W. E. (2006). Hazard analysis and visual effectiveness of the Surefire M6 Guardian. Technical Report AFRL-HE-BR-TR-2006-0048, Air Force Research Laboratory, Brooks City Base, TX 78235.

26. Early, E. A., Chavey, L. J., Rogers, B. Z., Kosnik, W. D., & Mitchell, W. E. (2006). Hazard analysis and visual effectiveness of the Peak Beam Systems Maxa Beam. Technical Report AFRL-HE-BR-TR-2006-0053, Air Force Research Laboratory, Brooks City Base, TX 78235.

27. AFRL/HEDO. (2003). Visual effectiveness analysis of the HAVESTAN laser system. Consultative Letter AFRL-HE-BR-CL-2003-0015, Air Force Research Laboratory, Brooks City Base, TX 78235.

28. Kosnik, W. D. (2008). Predicting transient visual deficits from low power laser illuminators. Technical Report AFRL-RH-BR-TR-2008-0021, Air Force Research Laboratory, Brooks City Base, TX 78235.

29. Smith, P. A., McLin, L. N., Stringham, J. M., Novar, B. J., Garcia, P. V., & Ahmed, E. M. (2012). Experimental validation of the photostress recovery model (PREMO). *Proceedings of the Directed Energy Professional Society*.

30. McLin, L. N., Novar, B. J., Smith, P. A., Garcia, P. V., Ahmed, E. M., Baker, T. J., & Huantes, D. F. (2014). Visual recovery for simple targets after broadband flash exposure Technical Report AFRL-RH-FS-TR-2014-0021, Air Force Research Laboratory, Fort Sam Houston, TX 78234.

31. McLin, L. N., Novar, B. J., Smith, P. A., Garcia, P. V., Ahmed, E. M., Baker, T. J., & Huantes, D. F. (2014). Visual recovery for complex targets after broadband flash exposure Technical Report AFRL-RH-FS-TR-2014-0013, Air Force Research Laboratory, Fort Sam Houston, TX 78234.

Appendix A: Software Architecture

Flashblindness.dll

This dynamically-linked, Win32 library written in ANSI C++ currently encapsulates the computational engine for computing the flashblindness (transient) effects of an optical source. This library depends on *NumericalRecipes.dll*.

NumericalRecipes.dll

NumericalRecipes.dll contains code based on the book "Numerical Recipes in C++". This code contains the convolution code required in the intraocular light scatter model. *Flashblindness.dll* also uses some of the base data types from *NumericalRecipes.dll*.

Open Scene Graph

The 3D functionality of the Vision Effects library is provided by an Open-Source Scene Graph library called OpenSceneGraph (OSG). OSG is an objected oriented interface to the OpenGL application programming interface that provides the 3D application programmer an Object Oriented interface that also provides most of the necessary infrastructure required for a 3D visual simulation. OSG makes the 3D environment more intuitive and object oriented and makes the scenes more efficient by limiting costly context switching in OpenGL. OSG also allows 3D model and image files of various formats to be read. The types of files that can be read are based on the available plug-ins. These plug-ins have the format *osgDB_*.dll*. Looking through the bin directory will reveal the types of models and images that can be loaded. Most importantly, this plug-in can load 3D models of the format **.3ds, *.lwo, *.lws, *.dxf, *.flt*, and **.osg*. It can load image files of the type **.bmp, *.jpeg, *.tiff*, and **.png*.

Client Applications

A plug-in for the AFRL/RHDO Application Framework, called *Flashblindness_Plugin.dll* was created to provide a more consistent and feature rich user interface. As the framework is a .NET application, the plug-in assembly/DLL was written in C#. An intermediate bridge library, *Flashblindness_Bridge.dll* was written in managed C++ to bridge managed and un-managed code.

Appendix B: Optical Radiation Sources

Optical sources can be either broadband or laser devices. Laser beam fluence is normally described in terms of W m^{-2} for CW exposures or J m^{-2} for pulsed exposures. However, for visual effects analysis, laser emission must be converted from radiometric to photometric units to account for the differential spectral sensitivity of the eye. The spectral luminosity function for photopic vision is shown in Figure 11. If laser fluence is specified by the user in radiometric units, the model converts to photometric units using the following method.

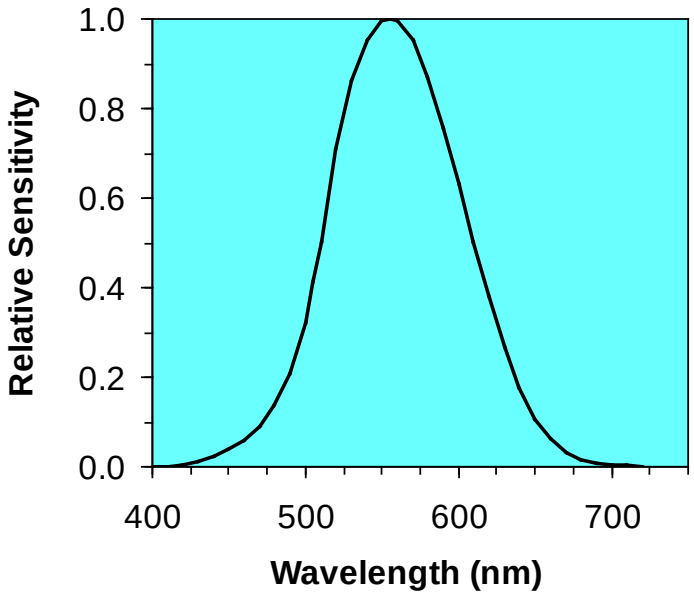

Figure A-1. The CIE photopic spectral luminosity curve. The curve shows that the strength of the response of the normal human eye depends on the incident wavelength. The eye's response is strongest to 555 nm under photopic or daylight conditions.

The photometric equivalent of irradiance is illuminance, E_v (in $lm \cdot m^{-2} \equiv$ lux), which is related to irradiance, E_e (in W m^{-2}), by:

$$E_v = 683 \times E_e \times V_\lambda \tag{1}$$

where 683 is the luminous efficacy constant in units of $lm \cdot W^{-1}$, and V_λ is the photopic spectral luminosity coefficient. In addition, since the human visual system perceives a flickering light source with a frequency above 60 Hz as continuous, the effects of pulsed laser systems with pulse repetition frequencies greater than 60 Hz can also be analyzed. For these pulsed sources, the irradiance is given by the time-averaged irradiance.

The above relation is the photometric conversion for CW sources for glare analysis. The flash recovery model is used to analyze the recovery of visual sensitivity after the source has been turned off. This model is generally appropriate for pulsed or short duration laser exposures. However, as with glare sources, multiple-pulse exposures greater than 60 Hz may also be analyzed as a single continuous pulse. For pulsed sources the relation involves the conversion

from radiant energy to time-integrated illuminance. The model accepts pulsed laser input in terms of a radiant exposure, H_e ($J \cdot m^{-2}$). The radiant exposure is converted to photometric units by the equation:

$$H_v = 683 \times H_e \times V_\lambda , \tag{2}$$

where H_v is the integrated illuminance in $lm \cdot m^{-2} \cdot s$.

Broadband optical sources are processed through a similar procedure except that the spectral and, if necessary, the spatial distribution of the source must be considered.

The eye is sensitive to optical radiation over a bandwidth of 400-700 nm. Therefore, the total source irradiance has to be calculated over this band. The model accepts a text file of the relative spectral distribution of the source. The text file has a two column format of wavelength number and relative intensity. The model truncates the distribution to the visible band and interpolates between wavelengths, if necessary. The user may also choose an appropriate spectral distribution based on blackbody color temperature from a built-in database if no spectral data are available.

The model uses the source or irradiance to scale the relative spectral distribution to spectral irradiance in terms of $W \cdot m^{-2} \cdot \lambda^{-1}$. The spectral irradiance, $E_{\lambda,}$ is weighted by the photopic luminosity coefficient at each wavelength, and is integrated across the visible band to obtain illuminance, $E_{v,}$ by:

$$E_v = 683 \times \int E_\lambda \times V_\lambda \times d\lambda , \tag{3}$$

where 683 is the luminous efficacy constant in units of $lm \cdot W^{-1}$ and V_λ is the photopic luminosity coefficient. The source illuminance E_v is then multiplied by the exposure duration t to obtain the integrated luminous exposure H_v in $lm \cdot m^{-2} \cdot s^{-1}$ for pulsed sources

$$H_v = E_v \cdot t . \tag{4}$$

If the source irradiance was measured at a distance other than the observation distance then the luminous exposure has to be corrected for viewing distance. For a source measured at a distance d, the inverse-square law is used to calculate the luminous exposure at the observation distance d_{of} and is given by

$$H_v(d_{of}) = H_v(d) \cdot \left(\frac{d}{d_{of}} \right)^2 . \tag{5}$$

Thus, the luminous exposure represents the total brightness of the source at the observation distance. In the case where the source is extended, that is occupies space, the luminous exposure must also be scaled by the physical area of the source. The physical area is defined by the user in terms of a length and a width. For uniform sources the luminous exposure is simply applied to the entire surface. However, for a non-uniform source the individual elements of the surface

must be calibrated by the total luminous exposure. This is accomplished by employing the user-supplied 2D spatial distribution or a pre-defined Gaussian spatial distribution supplied by the model. This distribution has parameters for both the horizontal and vertical directions. In one dimension, the distribution *g(x)* has the form:

$$g(x) = \exp\left(-(x - x_0)^2 \Big/ \sigma^2 \right), \tag{6}$$

where x_0 and σ are the center and the 1/e location of the distribution, respectively. Whether the flash distribution is supplied by the user or the model, the calibration procedure is the same. For an *m* x *n* array, where each element *i* represents the relative source intensity at that point in space, *i* is scaled by the ratio of the total luminous exposure to the sum of the relative intensities in the array to obtain the calibrated luminous exposure $H_{m,n.}$

$$H_{m,n} = \frac{i_{m,n} H_v}{\sum_{1}^{m,n} i} \quad . \tag{7}$$